# 圓鼻車刀當刀尖磨耗時車削不銹鋼材之切削力預測

## 張充鑫

國立宜蘭技術學院機械工程學系教授

## 摘　要

為了研究負稜主刃車刀當刀尖磨耗時，切削不銹鋼材的切削力量，刀尖溫度及主切屑與第二切屑的生成情形，一種新的切削力學模式在此建立。此模式伴隨著刀具在磨耗狀況下，切削不銹鋼時其產生的剪切面積變化以預測切削力，結果理論值與實際值很接近。

**關鍵詞**：不銹鋼、磨耗圓鼻刀具、負稜主刃、斜交車削及最小能量法

# Prediction of the Cutting Forces of Stainless Steel with Nose Radius Worn Tools

## Chung-Shin Chang

Professor Department of Mechanical Engineering, National Ilan Institute of Technology.

## Abstract

To study the cutting forces, the carbide tip's surface temperature, the mechanism of secondary chip and main chip formation of turning stainless steel with a chamfered main cutting nose radius worn tools. A new force model incorporating tool worn factor and using the variations of shear plane areas occurring in tool worn situations are presented in this paper. The results show a good agreement between the predicted and measured forces.

**Key words:** Stainless steel, nose radius worn tool, chamfered main cutting edge, oblique cutting, minimum energy method

# I. Introduction

In general, stainless steels are large in the viscosity, poor in the heat conductivity and are apt to be coherent to a tool in the cutting, so that they are difficult to be subjected to the cutting work [1]. The three characteristics of stainless steel that have the greatest influence on machinability are: its relatively high mechanical properties (including yield strength), its high work-hardening rate, and its ductility-which explains the materials tendency to form a built-up edge during machining [2]. Industrial developments have let to higher output, better finish, and lower cost of the machining of stainless steel. For example, tools with longer cutting lives, lower tooling costs and reduce downtime. New metal-removal methods can produce parts with smoother finishes and greater accuracy. Larger, more rigid, more powerful machines also aid in metal removal [3]. Zhu and others [4] demonstrated in the art of machining, cutting tools have gradually evolved from tools with a flat rake face to tools with complex rake face features including obstructions and grooves. Fuh and Chang [5] had developed a force model for nose radius tools with a chamfered main cutting edge. Sewailem & Mobarak [6] demonstrated that the wearing of a cutting tool is affected by many factors, e.g., materials, cutting conditions, geometry and cutting forces. Usui and Hirota [7, 8] used an iterative technique to find the chip flow direction that minimized the sum of the shear and friction energies. They calculated shear energy of a series of parallel effective shear planes (consisting of the cutting velocity and chip flow vector) along the active cutting edge. Shamoto and Altintas [9] demonstrated the mechanics of oblique cutting are defined by five expressions. Three of the expression is obtained from the geometry of oblique cutting, and applying either maximum shear stress or minimum energy principle derives the remaining two. For a given tool geometry average friction angle between the cutting tool and work material and average shear yield stress of work material, the proposed theories can predict the shear angles, chip flow direction and the direction of resultant force in oblique machining operation. Chang [10] showed a model for accurately predicting the cutting force for turning of stainless steel upon its wearing with a sharp chamfered main cutting edge tool was also developed. Analyzing the three dimensional cutting force when nose tool wear occurs has received extensive attentions. However, the effects of nose radius worn tools were excluded from his discussion. For predicting the correct cutting forces, however, shear plane areas must be cooperated with the wear effects of nose radius tool edge during the cutting process stainless steel. The objective of this paper is to set up a three-dimensional oblique cutting stainless steel models to study three-dimensional cutting operations for a round nose tool with a chamfered main cutting edge considering wear.

# II. Theoretical Analysis

A three dimensional cutting model with a single-point tool is a simplest case including main and front cutting edges. The simplest case including these two factors is shown in Fig 1. According to Fuh and Chang [11], a force model for nose radius worn tools with a chamfered main cutting edge, which can accurately predict the formations of shear planes for the case of chamfered main cutting edge, must have not only nose radius $(R)$, worn depth $d_B$, cutting depth $d$, feed rate $f$, cutting speed $V$, second side rake angle $a_{S2}$, and parallel back rake angle $a_b$, $C_s$ is the side cutting edge angle, $C_e$ is

the end cutting edge angle, $a_{S1}$ is the first side rake angle, $a_{S2}$ is the second side rake angle. $a_{S1}$ and $a_{S2}$ are used as shown in Table 1. The process for deriving the shear plane areas is divided into parts with tool wear and without wear.

## 1. Shear Areas in the Cutting Process with A Chamfered Main Cutting Edge Nose Radius (*R*), Tool Without Wear

The calculations of shear area $A$ and projected area $Q$ fall into one of the following categories depending on the relationship between nose radius, feedrate and the depth of cut.

**A.** The nose radius of the tool ($R$) and where the nose radius (*R)* is smaller than the feedrate (*f*), $R \neq 0$  $R < f$ , as shown in Fig. 1, the shear plane area $A$ includes the area of the triangle $A_1$, trapezoid area of $A_2$, secondary chip's $A_S$ and the cylindrical area $A_3$, formed by the tool nose radius [5].

**B.** Nose radius of the tool ($R$) is larger than the federate ( $f$ ), $R \neq 0$  $R > f$ , according to the depth of cutting, which can be subdivided into three parts: (a) $d > R$ , (b) $d = R$  and (c) $d < R$ , as shown in Ref. [5].  Because of either a small rate of feed or a larger nose radius, the shear plane area $A$ does not consist of the area of triangle $A_1$.

In this section we evaluate the case of small radius, that is case 1, $R \neq 0$  $R < f$  [5].

$$A = A_1 + A_2 + A_3 + A_s ,  \qquad (1), \quad Q = Q_1 + Q_2 + Q_3 . \qquad (2)$$

## 2. The Shear Areas A of the Cutting Process with A Chamfered Main Cutting Edge Nose Radius Worn Tool ( $R \neq 0, R < f$ )

According to Takeyama et al. [12] showed that determination of cutting force components is one approach to confirm the wear behavior of lathe tools during the cutting process.  Abdelmoneim et al. [13] have further suggested that the tool edge may in fact wear rapidly to form a cylindrical surface with a larger nose radius and an adjoining flat wear land. According to the last section (section **1.**), the calculation of shear area $A$  and the projected area $Q$  for nose radius tools with a chamfered main cutting edge [5], when wear is occurring, can also be divided into following three categories.

**A.** sharpness of the tool  ($R = 0$)  with wears, as shown in reference [10].

**B.** wear nose radius of the tool  ($R$)  is smaller than the feedrate  ($f$),  ($R \neq 0$ ,  $R < f$ ), as shown in Figs. 2 to 3, the shear plane  $A$  includes the area  $A = A_1 + A_2 + A_3 + A_4 + A_5 + A_s$

**C.** wear nose radius of the tool  ($R$)  is larger than feedrate  ($f$),  ($R \neq 0$ ,  $R > f$ ) according to the depth of cutting, which can be subdivides into three parts (a)  $d > R$ ,  (b)  $d = R$  and  (c)  $d < R$ .

According to the above division, case **A.** has been discussed in reference [10] already.  This paper will therefore focus on the case of small radius, i.e. case **B.**  However, an experiment has been performed to study the case of large nose radius cutting, i.e. case **C.**, the results of which will be presented in future.

## 3. The Area of Shear Plane *A* and the Friction Plane *Q* for the Case B. Can be Obtained As Follows:

For convenience of calculation, the shear plane must be projected in the plane perpendicular to the speed of cut, which makes the calculations and analysis much easier and saves the time required for calculations. Defining the chip flow angle in this perpendicular section as  $h_c'$ , we get the relation between  $h_c'$  and  $h_c$  on the tool face, (Appendix *A11*). According to the equation, in Appendix *A11*, the shear plane area can be varied by changing  $h_c$  in small increments.

In Fig. 4, geometrical wear of the cutting tool on the tool face is shown from the top view so as to define the type of wear on the tool edge: viz. a curve of radius  $R_3$ , a straight line and a curve of radii  $R_2$ ,  $R_1$ ( $R_1 = R_2$ ).  The side view of the worn tool is shown in Fig. 5; from which the flank wears and wear land can be readily realized.

The measurable values (i.e. $l_1$, $l_2$, $l_3$, $l_4$, $l_5$, $h_1$, $h_2$, $h_3$, and $h_4$) can be obtained by amplifying the tool-maker microscope drawing the circumference of the tool edge before the cut, and again drawing the same after wear has occurred. The geometrical lengths, radius of curve and curve angles of the worn tool are shown in Fig. 4 and can be obtained by the following equations:

$$NP = (h_4^2 + l_5^2)^{1/2} ; \quad CN = (h_3^2 + l_2^2)^{1/2} ; \quad \overline{MC} = (h_2^2 + l_3^2)^{1/2} ; \text{ and } \quad DM = (h_1^2 + l_4^2)^{1/2} \tag{3}$$

$$q_{R1} = \tan^{-1}(l_5/h_4) ; \quad q_{R2} = \tan^{-1}(l_2/h_3) ; \quad q_{MC} = \tan^{-1}(l_3/h_2) ; \text{ and } \quad q_{R3} = \tan^{-1}(h_1/l_4) \tag{4}$$

$$R_1 = NP/(2\sin q_{R1}) ; \quad R_2 = CN/(2\sin q_{R2}) \text{ and } R_3 = DM/(2\sin q_{R3}) ; (R_1 = R_2) \tag{5}$$

Due to the variations in $C_s$ and the different kinds of geometrical circumferences of tool edge, several different cutting conditions occur when the feed is varied. In order to understand the cutting conditions, a criterion for determining the critical length and critical feed are developed and are shown in Fig. 6. The critical feed $f_d$ and critical length $h_c$ are:

$$h_c = h\sin C_s - p\cos C_s / \sin(q_{MC} - C_s) \quad (6), \quad f_d = (h - h_c \cos q_{MC})/\cos C_s \tag{7}$$

$$p = R_1 \cos 2q_{R1} - R_2 \cos 2q_{R2} - R_3 \sin 2q_{R3} + l_1 + l_2 \quad (8), \quad h = R_1 \sin 2q_{R1} + R_2 \sin 2q_{R2} - R_3(1 - \cos 2q_{R3}) + h_3 + h_4 \tag{9}$$

Two conditions are developed for the cutting process. First the straight line $\overline{MC}$ is intersected by the curve $CP$ only. And second, the line $\overline{MC}$ is intersected by curve $CP$, or the curve $DM$ is intersected by curve $CP$. In the first case, wherein the straight line $\overline{MC}$ is intersected by curve $CP$, feedrate ($f$) can be divided into another two cases, depending on the cutting condition, as:

**A.** when condition $f > f_d$ occurs

**B.** when condition $f \leq f_d$ occurs

The present work only concerns the case **A.**, i.e. $f > f_d$. Future work is intended to extend the present analysis to case **B.**

For simplification of the calculations, the simplified model is shown in Fig. 6, in which the actual feed in Figs.7 and 8 have been modified. The length of $\overline{ZZ'}$ can be calculated from Fig. 7 as:

$$\overline{ZZ'} = hh/\sin(q_{MC} + C_e - C_s) \quad (10), \quad hh = (h_1 + h_2 + h_3 + h_4)\sin(C_e - C_s) + (l_3 + l_4)\cos(C_e - C_S)$$

$$-R_1 \cos 2q_{R1} + R_2 \cos 2q_{R2} \quad \cos(C_e - C_s) - f\sin C_e - R_3[1 + \sin(C_e - C_s) - 2q_{R3}] \tag{11}$$

The modified feed $f_{CD}$ is therefore calculated as:

$$f_{CD} = f\cos C_s + R_3(1 - \cos 2q_{R3}) + \overline{ZZ'}\cos q_{MC} \tag{12}$$

If $\overline{ZZ'} < 0$, i.e. the condition as shown in Fig. 8, the intersection angle $q_{IN}$ can be calculated as:

$$q_{IN} = C_e - C_s + \sin^{-1}(pp/R_3) , \text{ where,} \tag{13}$$

$$pp = (h_1 + h_2 + h_3 + h_4)\sin(C_e - C_s) + (l_3 + l_4)\cos(C_e - C_s) - (R_1 \cos 2q_{R1} - R_2 \cos 2q_{R2})$$

$$\cos(C_e - C_s) - f\sin C_e - R_3 \sin(C_e - C_s) \tag{14}$$

Thus yielding modified feed as:

$$f_{CD} = f\cos C_s + R_3(1 - \cos q_{IN}) \tag{15}$$

After the modified feed $f_{CD}$ is obtained, the shear plane area and the projected area on the tool face can be calculated from Fig. 9 as:

$$A = A_1 + A_2 + A_3 + A_4 + A_5 + A_s \quad (16). \quad \text{where,} \quad A_1 = 0.25[4a_1^2 n_1^2 - (a_1^2 + n_1^2 - c_1^2)^2]^{1/2} ; \tag{17}$$

$$A_2 = \frac{1}{\cos h_c} \int_0^{2q_{R2}} [f_{CD} - (h_1 + h_2) + h_3 - R_2 \sin(2q_{R2} - \Phi)]d_s + \int_0^{2q_{R1}} [f_{CD} - (h_1 + h_2 + h_3) + R_2 \sin(\Phi)]d_s ; \tag{18}$$

$$A_3 = \overline{MC}/\{2\cos h_c [2(f_{CD} - h_1) - h_2]\sin(h_c + q_{MC})const\} ; \tag{19}$$

3

$$A_4 = \int_0^{2q} R3\,[(f_{CD} + R_3\cos\Phi - R_3)/\cos h_c\,]d_s\ ;\ (20),\quad A_5 = 1/[2(i_1 + k_1)j_1 const1]\ ; \tag{21}$$

$$A_s = [W_e^2\cos^2 a_{s1}\tan C_s]/(2\sin f_e\cos a_b)\ \text{(as shown in Fig. 3)}. \tag{22}$$

The friction area on the tool face is derived as:

$$Q = Q_1 + Q_2 + Q_3\ (23).\quad Q_1 = [d/\cos C_s + (h_1 + h_2)\tan C_s]f_{CD} + 0.5(l_1 h_2 + l_2 h_3 - l_3 h_1 - l_3 h_2) + (l_2 h_4 - l_1 h_4 - l_3 h_1) -$$
$$R_1^2(2q_{R1} + 0.5f_{CD}^2\tan C_s) - 0.5\,[R_2^2(2q_{R2} - \sin 2q_{R2}) + 0.5R_3^2(2q_{R3} - \sin 2q_{R3}) - [l_1 - l_2 + 0.5\ (f_{CD} - h_1 - h_2 - h_3$$
$$-h_4)\ \tan C_s](f_{CD} - h_1 - h_2 - h_3 - h_4)\ ; \tag{24}$$

$$Q_2 = W_e\cos a_{S1}[(d/\cos C_s - W_e\cos a_{S1}\tan C_s)/\cos a_b] \tag{25}$$

$$Q_3 = (W_e^2\cos a_{s1}\tan C_s)/2\cos a_b\ .\ (Q_3\ \text{is the area of triangle}\ EE\overline{Y},\ \text{Fig. 3}) \tag{26}$$

The expressions for $a_1$, $c_1$, $e_1$, $g_1$, $i_1$, $j_1$, $k_1$, $n_1$, $const_1$, $\Phi$, $d_s$ and $h'_c$ are given in Appendix $A$

## 4. Calculation Flank Wear of A Worn Nose Radius Tool with Chamfered Main Cutting Edge

The wear of nose radius tool tip is shown in Fig. 10. The coordinates of points $O_1$, $C$, $S_2$, $M_1$ and $M$ are derived by using the data measured from optical microscope, as shown in the following:

$O_1$: $(X_{O1}, Y_{O1})=(R, R)$, M: $(X_M, Y_M)=(l_2 + l_5, h_1 + h_2)$, $C$:$(X_C, Y_C)=(l_2 + l_3 + l_5, h_1)$ and $S_2$: $(X_{S2}, Y_{S2})=(R - R\cos C_s, R - R\sin C_s)$. The coordinates of point $S_1$ can be obtained by establishing the equations for straight lines $\overline{O_1 S_2}$ and $\overline{MC}$, from which the point of intersection $S_2$ can be calculated, as, $S_2$: $(X_{S2}, Y_{S2})$

where

$$X_{S1} = \{[h_1 l_3 + h_2(l_2 + l_3 + l_5) - R_3 l_3]\cos C_s + R_3 l_3\sin C_s\}/[\overline{MC}\cos q_{MC} - C_S)] \tag{27}$$

$$Y_{S1} = \{[h_1 l_3 + h_2(l_2 + l_3 + l_5) - R_3 h_2]\sin C_s + R_3 l_4\cos C_s\}/\overline{MC}\cos q_{MC} - C_S) \tag{28}$$

Tool-edge wear in the direction of depth of cut has to be obtained in order to estimate the worn depth $d_B$ of the tool edge. The width of $\overline{MM}$ on the main cutting edge and $\overline{CC_1}$ on the front edge is also derived by establishing the relation between $\overline{MM}$, $\overline{CC_1}$ and flank wear. The length of $\overline{CC_1}$, $\overline{S_2 S_1}$, and $\overline{MM}$ are derived from following equations.

$$\overline{S_2 S_1} = [(X_{S1} - X_{S2})^2 + (Y_{S1} - Y_{S2})^2]^{\frac{1}{2}}\ (29),\quad \overline{CC_1} = h_1 - R + [R^2 - (R - l_3 - l_1 - l_5)^2]^{\frac{1}{2}}\ (30),\quad \overline{MM} = l_2 + l_5\ (31)$$

After the coordinates of tool face are derived, the worn depth of tool edge and flank wear of both main and front edge is determined by obtaining the relief angle (side relief angle, $q_{ref}$) and wear depth, $d_B$. From Figs. 11-13, the types of wear can be seen from the views of tool edge and that of main and front edges and a simple relation between flank wears $V_{B2}$, $V_{B3}$ and worn depth of the tool edge $d_B$ can be obtained.

$$d_B = \overline{S_2 S_1}\cos a_e\,(\cot q_{ref} - \tan a_e)\,(32),\ V_{B2} = \overline{MM}\,(\cot q_{ref1} - \tan a_{S2})\,(33),\ V_{B3} = \overline{CC_1}\,(\cot q_{ref2} - \tan a_e)\,(34),\ \text{where}$$

$q_{ref1}$ is the side relief angle on the main cutting edge (Fig. 12)

$q_{ref2}$ is the side relief angle on the front cutting edge (Fig. 13)

## 5. Cutting Forces Calculation

It is assumed that the energy is consumed as shear energy on the shear plane and as friction energy on the tool face. The shear energy per unit time ($U_s$) and the friction energy per unit time ($U_f$) were proposed by Usui et. al [7, 8] as:

$$U_s = F_s V_s = t_s AV\cos a_e/\cos(f_e - a_e)\ (\text{where}\ F_s = t_s A;\ V_s = (V\cos a_e)/\cos(f_e - a_e)) \tag{35}$$

$$U_f = F_t V_c = f_t\int_0^{B}d_b V_c = (t_s\sin bV\cos a_e Q)/[\cos(f_e + b - a_e)\cos(f_e - a_e)] \tag{36}\ \text{in which}$$

$$V_c = (V\sin f_e)/\cos(f_e - a_e)\ ,\ f_t = (t_s f\cos C_s\sin b)/[\cos(f_e - a_e + b)\sin f_e]\ (37),\ U = U_s + U_f = V(F_H)_{U\min}\ (38)$$

The values of shear areas with a worn nose radius tool, $A$, is calculated according to Eqs. (16)-(22), and the friction area $Q$ are calculated from Eqs. (23)-(26). The value of $a_e$ is determined according to equation (39). The experimental values of $a_e$, $b$, $f_e$, $t_s$ are obtained as follows. $b$ is the friction angle, which equals $\exp(0.848a_e - 0.416)$; $f_e$ is the effective shear angle and equals $(0.581a_e - 1.139)$ proposed by Usui [8]. $t_s$ is the shear stress, which equals to $571-19.9 a_e$ $MN/m^2$ (stainless steel) [10], and $h_C$ is the chip flow angle, which is determined by minimizing the total cutting energy $U$. Then it is necessary to calculate the effective rake angle $a_e$, and applying the equation (39) can attain it. The cutting force $F_H$ can be determined by applying the equation proposed $VF_H = U_s + U_f = U$ for $U_{\min}$ in conjunction with the energy method (R. E. M. method) [14] and V is the cutting speed. Therefore,

$$a_e = \sin^{-1}(\cos h_c \sin a_{S2} \cos a_b + \sin h_c \sin a_b) \tag{39}$$

$$F_H = (F_H)_{U\min} = \frac{U_{\min}}{V} = \{\frac{t_s \cos a_e A}{\cos(f_e - a_e)} + \frac{t_s \sin b \cos a_e Q}{[\cos(f_e + b - a_e)\cos(f_e - a_e)]}\} \tag{40}$$

$$(R_t)_H = (F_H)_{U\min} = (F_t)_{U\min} \sin a_e + N_t \cos a_b \cos a_{S2} \tag{41}$$

where the frictional force is determined by

$$F_t = (t_s \sin b \cos a_e Q)/[\cos(f_e + b - a_e)\sin f_e] \quad (42), \quad N_t = [(F_H) - (F_t)_{U\min} \sin a_e]/(\cos a_b \cos a_{S2}) \tag{43}$$

In Eq. (41), $(R_t)_H$ is the horizontal cutting force in the horizontal plane, $N_t$ is the normal force at the tip surface with minimum energy. Therefore, transverse cutting force, $F_T$, and vertical cutting force, $F_V$, can expressed by

$$F_T = -N_t \sin a_b \cos a_{S2} + F_t(\cos a_b \sin h_c - \sin a_b \sin a_{S2} \cos h_c) \quad (44), \quad F_V = -N_t \sin a_{S2} + F_t(\cos a_{S2} \cos h_c) \tag{45}$$

## 6. Modified Force Model for Worn Nose Radius Tool with Chamfered Main Cutting Edge

Due to the size effects, a modified cutting force model is presented in this paper to get more precise results. Besides the horizontal force $F_H$, the plowing force $F_P$, due to the effects of tool edge and wear force $F_W$, due to the effects of flank wear proposed by Fuh [5] are considered into the prediction of the modified horizontal cutting force $F_{MH}$, as illustrated in Ref. [10]. That is

$$F_{HH} = F_{MH} = (F_H)_{U\min} + F_P + F_W \tag{46}, \quad F_P = (HB)rL_{f1}, \tag{47}$$

where *HB* is the Brinell hardness of the workpiece, r is the radius on the main cutting edge between the face and flank.

$$F_W = t_y[(\overline{MC}d_B L_{f2} V_{B2})/2 \cos a_{S2} + L_{f3} V_{B3}] \tag{48}$$

$$L_{f1} = d/\cos C_S + (h_1 + h_2)\tan C_S - l_3 - l_4 + (2R_1 q_{R1} + \overline{MC} + 2R_2 q_{R2} + 2R_3 q_{R3})/\cos a_{S2} + [f_{CD} - (h_1 + h_2 + h_3 + h_4)]$$
$$/[\cos a_{s2} \cos(C_s - C_e)] \tag{49}$$

$$L_{f2} = 2R_3 q_{R3}/\cos a_{S2} + d/\cos C_s + (h_1 + h_2)\tan C_s - l_4 - l_3 \tag{50}$$

$$L_{f3} = 2(R_1 q_{R1} + R_2 q_{R2})/\cos a_{S2} + [f_{CD} - (h_1 + h_2 + h_3 + h_4)]/[\cos a_{S2} \cos(C_e - C_s)] \tag{51}$$

Where $L_{f1}$, $L_{f2}$ and $L_{f3}$ are the contact lengths between the cutting edge and workpiece, as shown in Fig. 4; $d_B$ is the tool worn depth (Fig. 11). $V_{B2}$ and $V_{B3}$ are the tool flank wear (shown in Figs. 12 and 13).

If the Brinell hardness of the workpiece, *HB,* is given, the expressions for r $s_y$, $t_y$ given by Cook [15], are listed as

$$s_y = \frac{HB}{p}, \tag{52} \quad \text{and} \quad t_y = \frac{s_y}{2} \tag{53}$$

The modified transverse cutting force $(F_T)_M$ is equal to the theoretical transverse cutting force, $F_T$; obtain from equation (44), plus a thrust force caused by tool wearing. This thrust force can be estimated by multiplying the worn surface area $(L_p V_B)$ by the yield strength of the workpiece $s_y$. The expression for $(F_T)_M$ is given in equation (54).

Similarly, the modified vertical cutting force $(F_V)_M$ is equal to the theoretical vertical cutting force $F_V$, as obtained from equation (45), plus a shear force caused by tool wearing. The shear force can be obtained by multiplying the worn surface area ($L_p V_B$) by the shear strength of the workpiece $t_y$. The expression of $(F_V)_M$ is given in equation (55).

$$(F_T)_M = F_T + [s_y d_B \overline{MC} \cos q_{MC} - C_s)]/2\cos a_{S2} + s_y[(L_{P1}V_{B2} + L_{P2}V_{B3})] \tag{54}$$

$$(F_V)_M = F_V + t_y[d_B \overline{MC} \cos q_{MC} - C_s)/2\cos a_{S2} + t_y(L_{P1}V_{B2} + L_{P2}V_{B3}) \tag{55}$$

$$L_{P1} = [2R_3 q_{R3} \cos q_{R3} + C_s)]/\cos a_{S2} + \quad d/\cos C_s + (h_1 + h_2)\tan C_s - l_4 - l_3]\sin C_s \tag{56}$$

$$L_{P2} = 2[(R_1 q_{R1} + R_2 q_{R2})\cos 2q_{R1} + 2q_{R2} + C_e - C_s)]/\cos a_{S2} + [f_{CD} - (h_1 + h_2 + h_3 + h_4)]/\cos C_e - C_s) \tag{57}$$

where, $L_{P1}$ and $L_{P2}$ are the projected contact lengths between the tool and workpiece, as shown in Fig. 4. According to figure 14, the final modified horizontal cutting force $F_{HH}$, transverse cutting force, $F_{TT}$, and vertical cutting force, $F_{VV}$, can be calculated by

rewritten for as follows:

$$F_{HH} = (F_H)_M = (F_H)_{U\min} \quad (58), F_{VV} = (F_V)_M \cos C_s - (F_T)_M \sin C_s \text{ (for } C_s \neq 0^-) \tag{59}$$

$$F_{TT} = (F_T)_M \cos C_s + (F_V)_M \sin C_s \text{ (for } C_s \neq 0^-) \tag{60}$$

# III.   Experimental Method and Procedure

To verify the developed present force model, experimental arrangement is set up, as shown in Fig 15. The machine tool used for the test is the *Victor, 600*700* (brand name) lathe. In Fig. 15, the workpiece is held in the chuck of the lathe and mounted the cutter on a dynamometer (Kistler type 9257B) to measure the three-axis component force. The force signals being recorded through charge amplifiers and $A/D$ converter. An infrared detector was used to monitor the cutting tips and the temperature can be stored in the computer. All the measured data was recorded by a data acquisition system (Keithley Metrobyte Das-1600) and analyzed by the control software (Easyest). To investigate the effects of various cutting geometries on the cutting force and the secondary chip formation, nine special cutting tool holders are used to obtain the specified side cutting edge angle, $C_S$, and the secondary side rake angle, $a_{S2}$. The tools specifications of nose radius, flank wear, relief angle, and first negative side rake angle and chamfer width are listed in Table 1. A total of 6 tool geometries are used in various combinations of tool holder and tips. The cemented carbide tips are ground on a tool grinder (Lion). and the dimensions of these tool holders and tool tips are inspected with a coordinate measuring machine (Mitutoyo B706) to verify that they met the specifications. The nose radius cutting tools were ground to a wear depth, after the wear land was measured from toolmakers microscope (Mitutoyo TF 510F), and the three-dimensional cutting forces were calculated accordingly.

The workpieces are stainless steel, SUS304 65 mm diameter; 500mm lengths cut from the same bar were used. The composition of workpiece was *C=0.05%, Mn=1.17%, P=0.34%, S=0.24%, Si=0.29%, Ni=9.14%, Cr=18.45%, 168HB.*

The cutting tools used in the experiments are Sandvik p10, type *S1P* [16]. Carbide-tipped tools having the following angles were used: Back rake angle=$0°$; side rake angle=$6°$; end relief angle =$7°$; side relief angle =$9°$; end cutting edge angle=$70°$; side cutting angle=$20°$, $30°$, $40°$, and nose radius=0.1, 0.3 mm. Tool composition: *WC 69%, TiC 15%, TaC 8%, Co 8%, HV =1740*, the tool geometries are summarized as Table 1;

The experimental tests are maintained at the same conditions as follows: dry cutting; cutting velocity equals to 140-148 m/min; cutting depth equals to 1 and 2 mm; feedrate equals to 0.33mm/rev; the tool holder is vertical to the workpiece; and protrusion of tool tip from the dynamometer is 30 mm. For each tool configurations, the workpiece was turned to be a length of 240 mm in the feed direction. The data were recorded three times at different sections. The average values will be taken. The shapes of the main and the secondary tips were observed. Block diagrams of performance are written as shown in Fig. 16.

# IV. Results and Discussion

## 1. The Cutting Forces

According to Eqs. (16) -(26), the shear area $A$ and projected area $Q$ of cutting cross section of the tool face with a chamfered main cutting edge nose radius tool considering wear can be calculated. After obtaining the values of the shear area $A$ and friction area $Q$, the shear energy per unit time $U_S$ and the friction energy per unit time $U_f$ can be calculated from Equations (35) to (36). The theoretical principal component of the cutting force $F_H$ can be obtained from Eqs. (40) and (41). Then the transverse theoretical cutting force $F_T$ can be calculated from Eqs. (42)-(44). When $C_S$ is not zero, the plowing force must be taken into account to obtain the modified three axis cutting forces $F_{HH}$, $F_{TT}$ and $F_{VV}$ (Fig. 14) by applying Eqs. (58)-(60). The values of the theoretical, modified and experimental results for each $F_{HH}$, $F_{TT}$ and $F_{VV}$ are plotted compared in Figs. 17-19. The computational flow chart is illustrated in Fig. 16. The results shown in the figures imply the following conclusion:

**A.** According to the investigations under a constant side cutting edge angle $C_S$ and nose radius, $R$ equals 0.3mm, Chang and Fuh [5] calculated that the increase of the side rake angles $a_{S1}$ and $a_{S2}$ results in the decrease of cutting force $F_{HH}$ and $F_{VV}$. The reason is that the areas of shear and friction are decreased, and the contact length between the cutting edge of tool and the workpiece are decreased, whereas the effective rake angle and effective shear angle are decreased. However, for $C_S$ equals 20⁻, an increase of $a_{S1}$ and $a_{S2}$, increased the cutting force $F_{TT}$. The reason was that the contact length between the cutting edge of tool and the workpiece were increased.

**B.** Figs. 17, 18 and 19 indicates that among the experimental, modified and theoretical horizontal, vertical and transverse cutting forces, there are a good agreement between the experimental values and modified results, for the wear tool geometries, $C_S = 30⁻$, ($a_{S1} = -10⁻$, $a_{S2} = 10⁻$, $l_1 = 0.02$, $l_2 = 0.082$, $l_3 = 0.137$, $l_4 = 0.235$, $l_5 = 0.01$, $h_1 = 0.078$, $h_2 = 0.147$, $h_3 = 0.211$, $h_4 = 0.02$); ($a_{S1} = -20⁻$, $a_{S2} = 20⁻$, $l_1 = 0.015$, $l_2 = 0.097$, $l_3 = 0.156$, $l_4 = 0.188$, $l_5 = 0.012$, $h_1 = 0.082$, $h_2 = 0.138$, $h_3 = 0.22$, $h_4 = 0.05$); ($a_{S1} = -30⁻$, $a_{S2} = 30⁻$, $l_1 = 0.03$, $l_2 = 0.102$, $l_3 = 0.168$, $l_4 = 0.205$, $l_5 = 0.018$, $h_1 = 0.058$, $h_2 = 0.14$, $h_3 = 0.248$, $h_4 = 0.0824$), at $q_{ref} = 6⁻$, $q_{ref1} = 7⁻$, V=140m/min, and $R = 0.3$ respectively.

**C.** The experimental, modified and theoretical values, both with and without tool wear, are compared for the same cutting conditions but different tool geometries, $C_S = 30⁻$, $a_{S1}(a_{S2}) = -10⁻(10⁻)$, $a_{S1}(a_{S2}) = -20⁻(20⁻)$ and $a_{S1}(a_{S2}) = -30⁻(30⁻)$, in Figs. 17 (a, b) and 19 (a, b). It can be seen that the values of three-dimensional cutting forces are larger by about 20% in case of tool wear as compared to those without tool wear.

**D.** The transverse cutting force, $F_{TT}$, increase greatly when tool wear occurs but the vertical force, $F_{VV}$, and horizontal cutting force, $F_{HH}$ does not. This is due to the effect of larger contact area of the tool's tip edge or the larger normal and larger stress on the tool's worn edge, hence $F_{TT}$ increase greatly.

## 2. Shape of the Chips

The relationship between secondary chip and the different tool geometries with various side rake angles and cutting edge angles when wearing has occurred are required. According to the cutting tests described in the previous section, Figs. 20(a, b and c), show photographs of the chips obtained by nine different tool holders when the nose radius of tips is taken as 0.3mm, and the side rake angles are $10^-$, $20^-$ and $30^-$ respectively. It can be observed from the experimental cutting chips, and the following phenomenon can be observed.

**A.** It is rather difficult to produce a secondary chip with the conditions of $C_s = 30^-$, $a_{S1} = -10^-$, and $a_{S2} = 10^-$. The smaller the side rake angle is, $a_{S1}$ and $a_{S2}$, the fewer the secondary chips produced. This inverse relation is due to both the effective side-rake angle and effective rake angle which are the smallest; however the friction angle is the largest and the secondary chip flows with more difficulty.

**B.** Although tool wear occurs, the secondary chip is still formed more clearly and flows more easily for conditions of $a_{S1} = -30^-$, $a_{S2} = 30^-$, and compared with the other conditions of $a_{S1} = -10^-$, $a_{S2} = 10^-$ and $a_{S1} = -20^-$, $a_{S2} = 20^-$.

## 3. Temperature of Tips

Hoshi et al. [17] concluded that the SWC tool could decrease the specific energy by 15%, and the lower cutting forces would result in lower temperatures in the main chip. Fig. 21 depicts plot of the tip temperature versus various side cutting edge angle ($C_s$) with the values of side rake angle ($a_{S1}$ and $a_{S2}$) for a worn tool with chamfer main cutting edge. From Fig. 21, it can be concluded that the tip's surface temperature does not exceed over 205 $^-C$ as a worn nose radius tool is used in turning stainless steel.

# V. Conclusions

We observed good correlation between predicted values and experimental results for cutting stainless steel forces when machining with sharpness of tools. Including the variation of shear plane areas has developed the new tool-worn model with chamfered main cutting edge. In this model, the energy method is also used to accurately predict a three-dimensional cutting stainless steel force considering tool wear. This model can be extended to on-line control domain in addition to the factors of time and thermal effect. Further work will extend to the analysis for nose radius tools.

The above results demonstrate that the predicted values correlated very well with the experimental values. Additionally, the new tool-worn model from using the variation of shear areas that occur in tool wearing conditions can be applied to accurately predict the cutting forces.

# References

(1) A. Kimura and N. Shibata (1989), Austenitic Free Cutting Stainless Steels, pp. 1-8, USPTO, No: 4837108, U.S.A.

(2) C. A. Divine JR. (1975), What to Consider in Choosing An Alloy, pp.19-23, Machining Stainless Steels, Published by the American Society for Metals (ASM), U.S.A.,

(3) D. G. Kligensmith (1975), New Processes, Alloys, Fluids Make Job Easier, Machining Stainless Steel, pp. 12-13 American Society for Metals .

(4) R. Zhu, S.G. Kapoor, R.E. DeVor and S.M.Athavale (1999), ''Mechanistic Force Models for Chip Control Tools'', Vol. 121, Trans., ASME, J. of Manufacturing Science and Engineering, pp. 408~416.

(5) Fuh and Chang (1995), Prediction of the Cutting Forces for Chamfered Main Cutting Edge Tools, Int. J. of Machine Tools and Manufacture, Design, Research, and Application, Vol. 35, pp. 1559~1586.

(6) M. R. Sewailem and I. M. Mobarak (1981), "The Pactical Estimation of Tool Wear in Turning", Wear, Vol. 67, pp.261-269.

(7) E. Usui and A. Hirota (1978), "Analytical Prediction of Three-Dimensional Cutting Process, part 2, Chip Formation and Cutting Forces with Conventional Single-Point Tool", Trans. ASME, J. of Engineering for Industry, Vol. 100, pp. 229-235.

(8) E. Usui, A. Hirota and M. Masuko (1978), "Analytical Prediction of Three-Dimensional Cutting Process, part 1, Basic Cutting Model and Energy Approach", Trans., ASME, J. of Engineering for Industry, Vol. 100, pp. 222-228.

(9) E. Shamoto and Y. Altintas (1999), Prediction of Shear Angle in Oblique Cutting with Maximum Shear Stress and Minimum Energy Principles, Trans., ASME, J. of Manufacturing Science and Engineering, Vol. 121, pp. 399-407.

(10) C. S. Chang (1998), "Turning of Stainless Steel with Worn Tools Having Chamfered Main Cutting Edges", Int. J. of Machine Tools and Manufacture, Design, Research, and Application, Vol. 38, pp. 291~313.

(11) K. H. Fuh and C. S. Chang (1998), "A Force Model for Nose Radius Worn Tools with A Chamfered Main Cutting Edge", Int. J. of Machine Tools and Manufacture, Design, Research, and Application, Vol. 38, pp. 1467~1498.

(12) H. Takeyama, H. Sekiquchi and K. Takada (1969), "One Approaching for Optimizing Control in Metal Cutting", Annals of the CIRP, Vol. 17, pp. 211-234.

(13) M. Es. Abdelmoneim and R. F. Scrutton (1973), "The Tribology of Cutting Tools During Finish Machining ", Wear, Vol. 25, pp. 45-53.

(14) A. Ravindran, G. V. Reklaitis and K.M. Ragsdell, Region-Elimin. Method (1984), Engineering Optimization, Methods and Applications, pp.37-46, published by Wiley- Interscience, New York, U.S.A.

(15) N. H. Cook (1969), The Mechanics of Chip Formation, in: Manufacturing Analysis, pp.37, published by Addison-Wesley Co. Inc., Reading, MA.

(16) K. J. A. Brookes (1992), World Directory and Handbook of Hard metals, pp. D172-175, 5th edition, published by International Carbide Data Handbook, United Kingdom.

(17) K. Hoshi and T. Hoshi (1969), SWC Cutting Tools in Metal Cutting Technology; pp. 87-104, Kogyo Chosakai Pub. Co., Ltd., Japan.

## Acknowledgments

91    08    02
91    08    28

## Nomenclature

$F_{HH}$      final modified horizontal cutting force.

$F_P$      plowing force ( $N$ )

$F_S$      shear force ( $N$ )

9

$F_{TT}$          final modified transverse cutting force.

$F_{VV}$          final modified vertical cutting force

$F_W$          additional force due to wear ($N$)

$L_f$          length of contact between tool and workpiece ($mm$)

$L_p$          projected length of contact between tool and workpiece ($mm$)

$r$          main cutting edge radius ($mm$)

$t$          flank wear length ($mm$)

$t_W$          depth of tool wear ($mm$)

$U_f$          friction energy ($N - m/\min$)

$U_{\min}$          minimum energy ($N - m/\min$)

$U_s$          shear energy ($N - m/\min$)

$W_e$          chamfering width ($mm$)

$a_{S1}$          first negative normal side rake angle ($rad$)

$f_B$          tool tip angle ($rad$)

$f_e$          effective shear angle ($rad$)

# Appendix *A*

**1. Coefficients of the Tool with Nose Radius ($R \neq 0$, $R < f$) with Wear Are:**

$$a_1 = 0.5\{f_{CD} - (h_1 + h_2) - R_2 \sin 2q_{R2} - R_1 2q_{R1} - R_2 \sin(C_e + C_s) - 2R_2 \tan[(C_e - C_s)]\}$$

$$\{\cos^2 a_e + [\tan a_{s2} \sin a_b + \tan(C_e - C_s)]^2 \cos^2 a_b\}^{1/2}/(\cos a_{s2} \cos a_b) \tag{A1}$$

$$c_1 = (e_1^2 + g_1^2 - 2e_1 g_1 \sin a_b)^{1/2} \text{ (A2)}, \quad j_1 = f_{CD} \text{ (A3)}, \quad k_1 = d/\cos C_s + (l_1 + l_2)\tan C_s - h_1 - h_2 \tag{A4}$$

$$e_1 = \{f_{CD} - (h_1 + h_2) - [R_1 2q_{R1} + R_2 \sin 2q_{R2} - R_2 \sin(C_e + C_s) - 2R_2 \tan(C_e - C_s/2)]\}$$

$$\{\tan h_c \cos a_b - [\tan a_{s2} \sin a_b + \tan(C_e - C_s)]\cos a_{s2}\}/(\cos a_{s2} \cos a_b) \tag{A5}$$

$$g_1 = \{[f_{CD} - (h_1 + h_2) - R_2 \sin(C_e - C_s) - R_2 2q_{R2} - R_1 2q_{R1} + R_2(C_e - C_s)] [\cos f_e \tan a_e]\}/\cos h_c \tag{A6}$$

$$i_1 = d/\cos C_s - \{l_4 + l_3 - l_2 - l_1 - (h_1 + h_2)\tan h_c + f_{CD}[\tan h_c - \tan(C_e - C_s) - \tan C_s] -$$

$$(h_1 + h_2 + h_3 + h_4)\tan(C_e - C_s)\} \tag{A7}$$

$$n_1 = [f_{CD} - (h_4 + h_3) - R_2 \sin(C_e - C_s) - R_2 2q_{R2} - R_1 2q_{R1} + R_2(C_e - C_s)] /(\cos h_c \sin f_e) \tag{A8}$$

$$const_1 = \{\cos^2 a_{s2} - \sin^2 f_e[\tan h_c \cos h_c - \cos a_{s2} \cos a_b(\cot f_e + \tan a_b)]^2\}^{1/2} /(\sin f_e \cos a_{S2} \cos a_b) \tag{A9}$$

$$\Phi = 0.5p + C_e + C_s \text{ (A10)}, \quad h_c' = \tan^{-1}[(\tan h_c - \sin a_{S2} \tan a_b)\cos a_b]/\cos a_{s2}, \tag{A11}$$

$$d_s = R\{\cos^2(h_c - \Phi) + [\cos f_e \sin(h_c - \Phi)\sin f_e/\sin f_e + \{\sin f_e(\sin a_b \cos \Phi - \tan a_{s2}(\sin^2 a_b + 1)\sin f)]^2\}^{1/2} \tag{A12}$$

Fig. 1 Detailed model of the chamfered main cutting edge nose radius tool without wear, $f > R$, $(R \neq 0)$



Fig. 2 Model of the chamfered main cutting edge nose radius tool considering wear occurs, $f > R$, $(R \neq 0)$
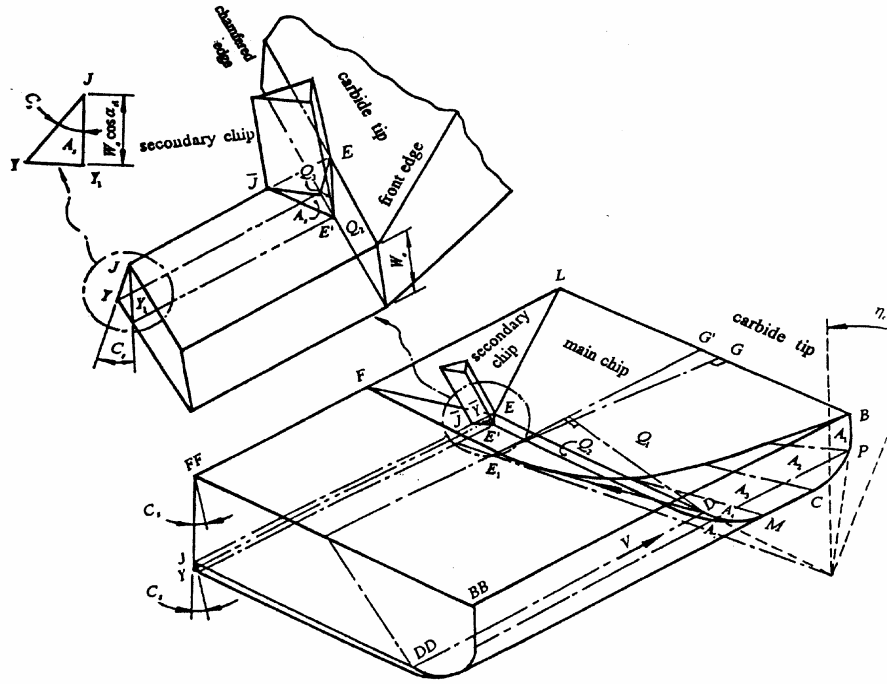
Fig. 3 Detailed model of the chamfered main cutting edge nose radius tool with wear, $f > R$, $(R \neq 0)$
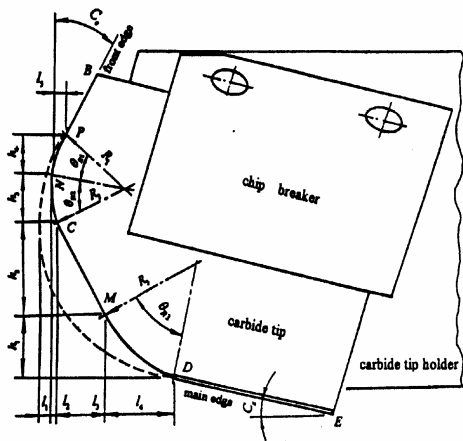


Fig. 4 Geometries of nose radius with wear
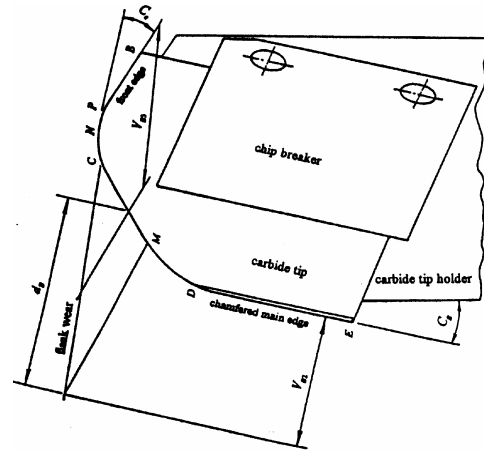
Fig. 5 The condition of wear for nose radius tool tip

12
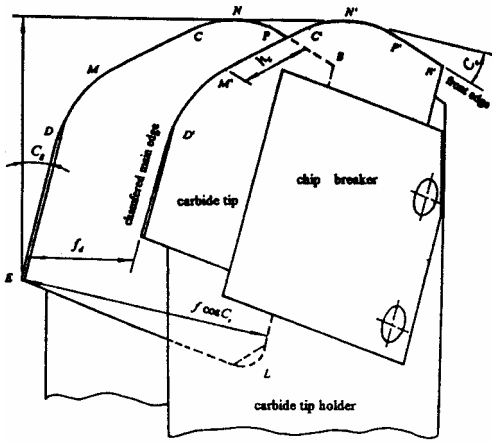
Fig. 6  The critical feed $f_d$, and the critical length $h_c$ of the worn tool
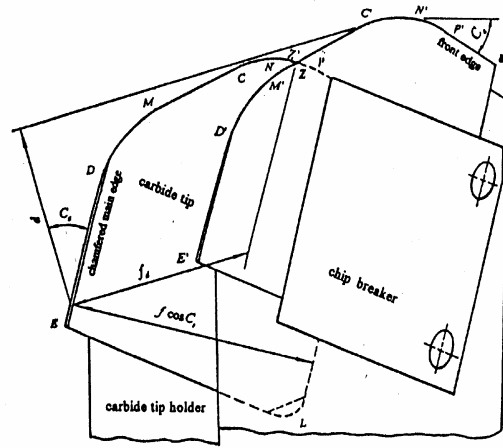


Fig. 7  The modified feed $f_{CD}$, when $\overline{MC}$ is intersected by the curve $CP$
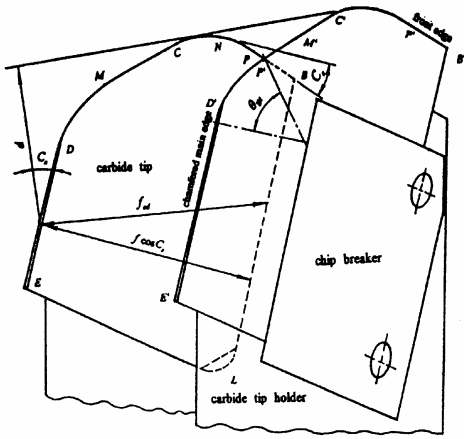


Fig. 8  The modified feed $f_{CD}$, when curve $DM$ is intersected by the curve $CP$
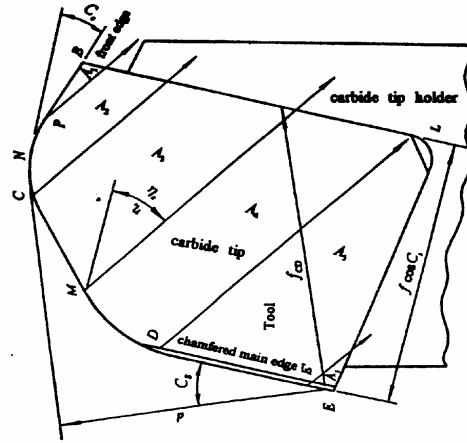


Fig. 9  The shear plane area $A$ and projected area $Q$ on the tool face when $f > f_{CD}$
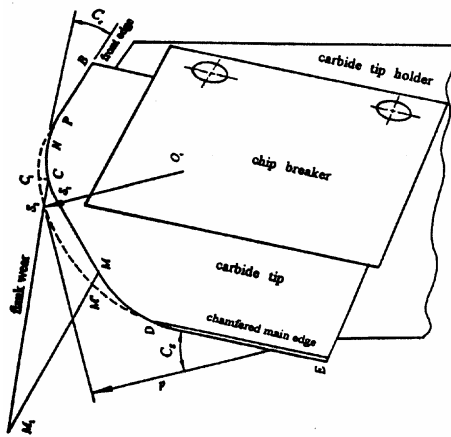


Fig. 10  The flank wear of a worn nose radius tool with chamfered main cutting edge
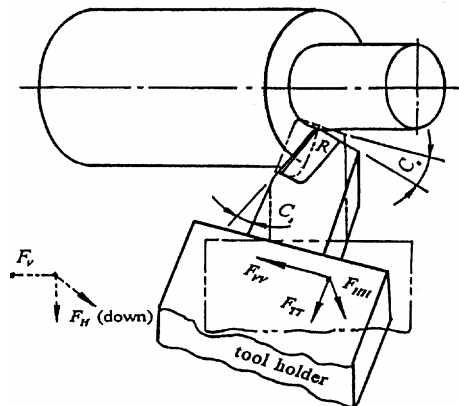


Fig. 14  Rotation of main cutting edge and positive directions of force components (final cutting forces)

13
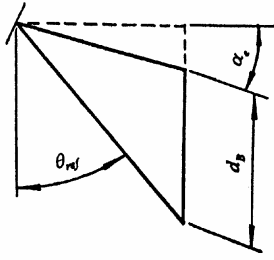
Fig. 11 Side relief angle $q_{ref}$, from the cross section of the tool tip in Fig. 10
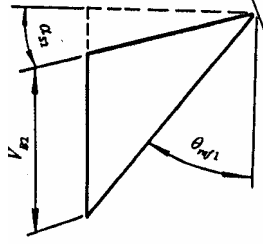
Fig. 12 Side relief angle $q_{ref1}$, from the cross section of the chamfered main edge in Fig. 10
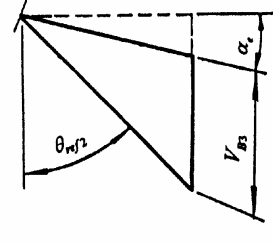
Fig. 13 Side relief angle $q_{ref2}$, from the cross section of the front cutting edge in Fig. 10



1. Workpiece ( JIS-S304C)
2. Tool (Insert tip, Sandvik-P10)
3. Accelerator (Kistler-8632B)
4. Dynamometer (Kistler-9257B)
5. Thermo-Hunter (NB-SH30A)
6. Charge Amp. (Kistler-5807A)
7. A/D converter (Metro Byte-STA160)
8. PC/CRT (V Time DX4-100)
9. Easyest Data Acquisition
10. Lathe (Vector-600*700)
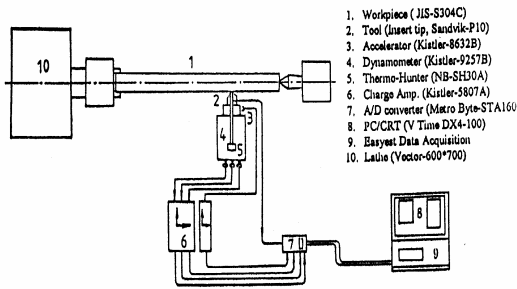
Fig. 15 Experimental set-up
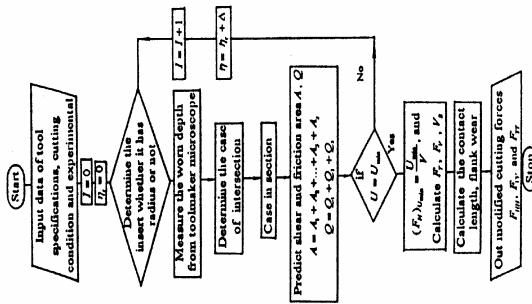
Fig. 16 Block diagram for predicting cutting force

(b-1) $\alpha_{S1} = -10°$     (b-2) $\alpha_{S1} = -20°$     (b-3) $\alpha_{S1} = -30°$     (a)
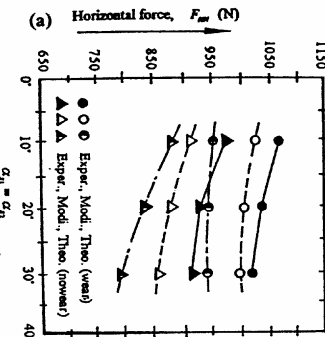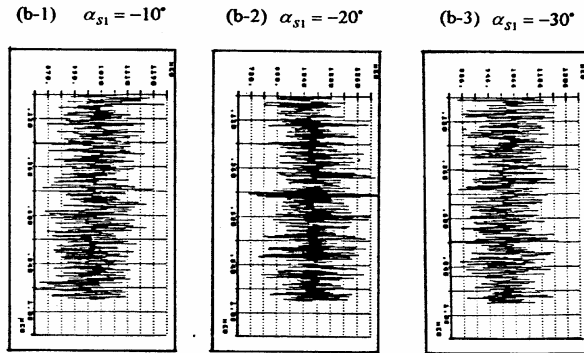


Fig. 17 Experimental, modified and theoretical horizontal cutting forces, (a) under wear as $l_1 = 0.02$, $l_2 = 0.082$, $l_3 = 0.137$, $l_4 = 0.235$, $l_5 = 0.01$, $h_1 = 0.078$, $h_2 = 0.147$, $h_3 = 0.211$, $h_4 = 0.02$, and no wear at $C_S = 30°$, $R = 0.3$, d=2mm, $f = 0.33$ mm/rev, $V = 148$ m/min for various $a_{S1}$ and $a_{S2}$ respectively, (b)((b-1), (b-2), (b-3)) experimental horizontal cutting force under wear as the same cutting conditions at $a_{S1}(a_{S2}) = -10°(10°)$, $a_{S1}(a_{S2}) = -20°(20°)$ and $a_{S1}(a_{S2}) = -30°(30°)$ respectively
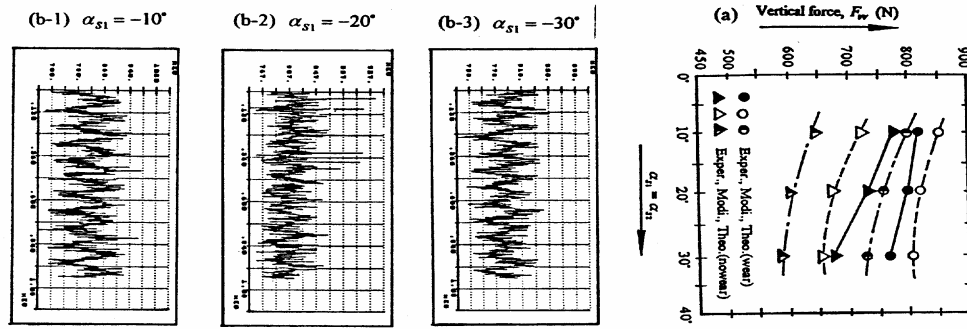
Fig. 18 Experimental, modified and theoretical vertical cutting forces, (a) under wear as $l_1 = 0.015$, $l_2 = 0.097$, $l_3 = 0.156$, $l_4 = 0.188$, $l_5 = 0.012$, $h_1 = 0.082$, $h_2 = 0.138$, $h_3 = 0.22$, $h_4 = 0.05$, and no wear at $C_S = 30^-$, $R = 0.3$ mm, d=2mm, $f = 0.33$ $mm/rev$ $V = 148$ $m/\min$ for various $a_{S1}$ and $a_{S2}$ respectively, (b)((b-1), (b-2), (b-3)) experimental vertical cutting force under wear as the same cutting conditions at $a_{S1}(a_{S2}) = -10^-(10^-)$, $a_{S1}(a_{S2}) = -20^-(20^-)$ and $a_{S1}(a_{S2}) = -30^-(30^-)$ respectively
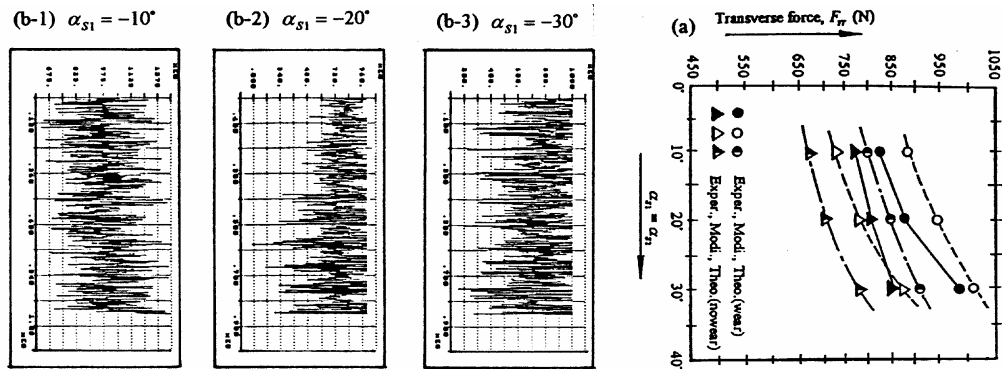


Fig. 19 Experimental, modified and theoretical transverse cutting forces, (a) under wear as $l_1 = 0.03$, $l_2 = 0.102$, $l_3 = 0.168$, $l_4 = 0.205$, $l_5 = 0.018$, $h_1 = 0.058$, $h_2 = 0.14$, $h_3 = 0.248$, $h_4 = 0.082$, and no wear at $C_S = 30^-$, $f = 0.33$ $mm/rev$, $R = 0.3$, d=2mm, $V = 148$ $m/\min$ for various $a_{S1}$ and $a_{S2}$ respectively, (b)((b-1), (b-2), (b-3)) experimental transverse cutting force under wear as the same cutting conditions at $a_{S1}(a_{S2}) = -10^-(10^-)$, $a_{S1}(a_{S2}) = -20^-(20^-)$ and $a_{S1}(a_{S2}) = -30^-(30^-)$ respectively
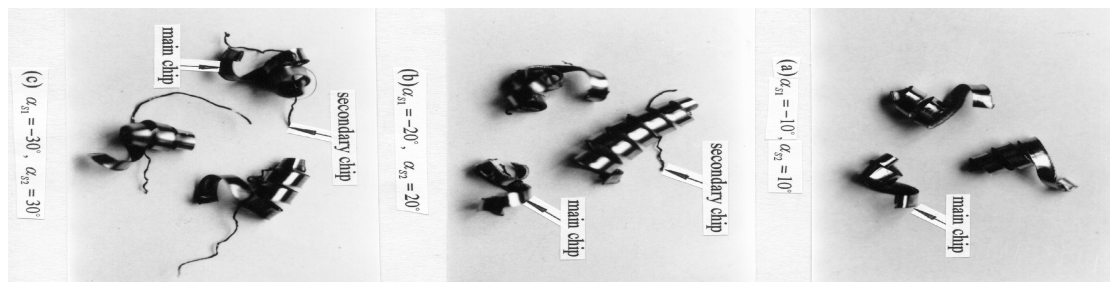


Fig. 20 The main and secondary chips with $C_S = 30^-$, both with wear tools as (a)$a_{S1} = -10^-$, $a_{S2} = 10^-$, $l_1 = 0.02$, $l_2 = 0.082$, $l_3 = 0.137$, $l_4 = 0.235$, $l_5 = 0.01$, $h_1 = 0.078$, $h_2 = 0.147$, $h_3 = 0.21$, $h_4 = 0.02$, (b) $a_{S1} = -20^-$, $a_{S2} = 20^-$, $l_1 = 0.015$, $l_2 = 0.09$, $l_3 = 0.156$, $l_4 = 0.188$, $l_5 = 0.012$, $h_1 = 0.082$, $h_2 = 0.138$, $h_3 = 0.224$, $h_4 = 0.05$ and (c) $a_{S1} = -30^-$, $a_{S2} = 30^-$, $l_1 = 0.03$, $l_2 = 0.102$, $l_3 = 0.168$, $l_4 = 0.205$, $l_5 = 0.018$, $h_1 = 0.058$, $h_2 = 0.14$, $h_3 = 0.248$, $h_4 = 0.082$ at $f = 0.33$ $mm/rev$, $R = 0.3$, d=2mm and $V = 148$ $m/\min$ respectively

15
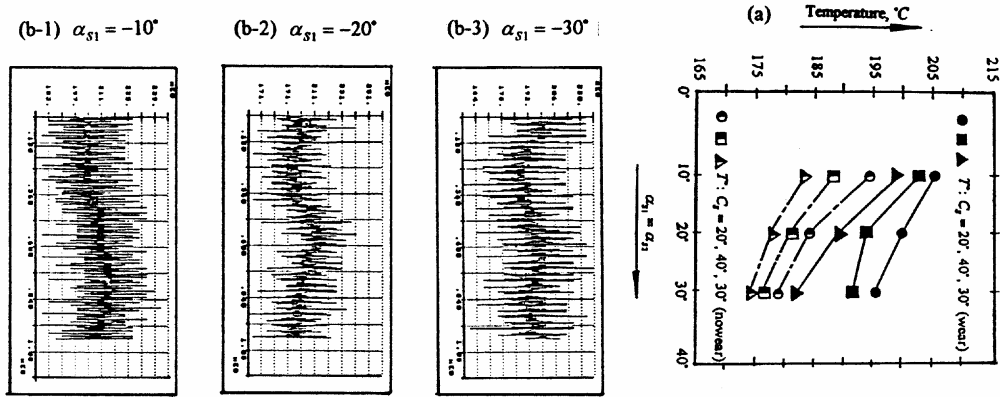
Fig. 21 Experimental values of temperature as (a) under wear ($C_S = 20^-$, $l_1 = 0.02$, $l_2 = 0.079$, $l_3 = 0.205$, $l_4 = 0.25$, $l_5 = 0.016$, $h_1 = 0.07$, $h_2 = 0.184$, $h_3 = 0.24$, $h_4 = 0.062$), ($C_S = 30^-$, $l_1 = 0.015$, $l_2 = 0.097$, $l_3 = 0.156$, $l_4 = 0.188$, $l_5 = 0.012$, $h_1 = 0.082$, $h_2 = 0.138$, $h_3 = 0.22$, $h_4 = 0.05$) and ($C_S = 40^-$, $l_1 = 0.015$, $l_2 = 0.11$, $l_3 = 0.22$, $l_4 = 0.053$, $l_5 = 0.011$, $h_1 = 0.044$, $h_2 = 0.135$, $h_3 = 0.252$, $h_4 = 0.062$), and no wear at, $f = 0.33$ $mm/rev$, $R = 0.3$, d=2mm and $V = 148$ $m/\min$, for various $a_{S1}$ and $a_{S2}$ respectively, (b)((b-1), (b-2), (b-3)) experimental temperature under wear as as the same cutting conditions at various $a_{S1}(a_{S2})$

Table   1.1    Tool geometries   specifications

| lead angle(side cutting edge) $C_s$ | tools No. | radial angles (side rake angles) $\alpha_{r1}$, $\alpha_{r2}$ ($\alpha_{r1}$, $\alpha_{r2}$) | nose roundness $R$ |
|---|---|---|---|
| 20° | 1 | 30°, −30° | 0.3mm (wear) |
|  | 2 | 30°, −30° | 0.3mm (no wear) |
| 30° | 3 | 30°, −30° | 0.3mm (wear) |
|  | 4 | 30°, −30° | 0.3mm (no wear) |
| 40° | 5 | 30°, −30° | 0.3mm (wear) |
|  | 6 | 30°, −30° | 0.3mm (no wear) |
| notation: tool holder and tips |  | | |

16